Styrene–Butadiene Rubber/Natural Rubber Blends: Morphology, Transport Behavior, and Dynamic Mechanical and Mechanical Properties

SONEY C. GEORGE,[1,*] K. N. NINAN,[2] GABRIEL GROENINCKX,[3] SABU THOMAS[1]

[1] School of Chemical Sciences, Mahatma Gandhi University, Priyadarshini Hills P. O., Kottayam, 686 560, Kerala, India

[2] Propellant and Special Chemicals Group, Vikram Sarabhai Space Center, Thiruvananthapuram, Kerala, India

[3] Laboratory of Macromolecular Structural Chemistry, Department of Chemistry, Katholieke University, Leuven, B-3001, Heverlee, Belgium

Received 8 March 1999; accepted 1 March 2000

ABSTRACT: Blends of styrene–butadiene rubber (SBR) and natural rubber (NR) were prepared and their morphology, transport behavior, and dynamic mechanical and mechanical properties were studied. The transport behavior of SBR/NR blends was examined in an atmosphere of *n*-alkanes in the temperature range of 25–60°C. Transport parameters such as diffusivity, sorptivity, and permeability were estimated. Network characterization was done using phantom and affine models. The effect of the blend ratio on the dynamic mechanical properties of SBR/NR blends was investigated at different temperatures. The storage modulus of the blend decreased with increase of the temperature. Attempts were made to correlate the properties with the morphology of the blend. To understand the stability of the membranes, mechanical testing was carried out for unswollen, swollen, and deswollen samples. © 2000 John Wiley & Sons, Inc. J Appl Polym Sci 78: 1280–1303, 2000

Key words: polymer blends; styrene-butadiene rubber; natural rubber; morphology; transport behavior; dynamic mechanical properties

INTRODUCTION

The scientific and commercial progress in the area of polymer blends during the past decades has been tremendous and was driven by the realization that, by blending, new materials can be developed and can be implemented more rapidly and economically. The question of whether two polymers are miscible is of paramount importance as far as their various properties are considered. The permeation properties of polymer blends depend mainly on the miscibility between two polymers. The blends may be heterogeneous or homogeneous. In homogeneous blends, the permeability is affected by the interaction between the component polymers,[1–3] while for heterogeneous blends, interfacial phenomena and the rubbery or glassy nature of the phases are important.[4]

Cabasso et al.[5] studied the diffusion of benzene–cyclohexane mixtures through polymer blends composed of polyphosphonates and acetyl cellulose. The blends are found to selectively absorb benzene from benzene–cyclohexane mixtures. Schori and Jagur-Grodzinski[6] described the permselective properties of blends of poly(vinyl pyrrolidone) (PVP) and a crown ether copolymer. The eight-membered crown ether ring strongly absorbs sodium salts from aqueous solu-

Correspondence to: S. Thomas.
**Present address:* Department of Polymer Technology, Crescent Engineering College, Seethakathi Estate, Vandalur P.O. Chennai 600048, India.

Journal of Applied Polymer Science, Vol. 78, 1280–1303 (2000)

tions. The introduction of hydrophilic PVP into the blend structure significantly increased the water permeability of the resulting blends. Aminabhavi and Phyde[7] studied the transport properties of a polymer blend consisting of the ethylene–propylene copolymer and isotactic polypropylene in haloalkanes. Aminabhavi and Phyde[8] investigated the sorption of aliphatic esters through tetrafluoroethylene/propylene copolymeric membranes. The results show that the diffusion coefficients, permeation coefficients, and kinetic rate constants decrease with increase in the size of the esters. Recently, in this laboratory, a series of transport studies were conducted based on natural rubber/epoxidized natural rubber,[9] the nitrile rubber/ethylene–vinyl acetate copolymer,[10] natural rubber/polystyrene,[11] and nitrile rubber/polypropylene[12] blends.

Styrene–butadience rubber (SBR) is a general-purpose synthetic rubber which has many applications. The high filler-loading capacity, good flex resistance, crack-initiation resistance, and abrasion resistance of SBR make it useful in several engineering and industrial applications. Natural rubber (NR) is a well-known polymer that has been widely used in a variety of industrial and engineering applications. The strain-induced crystallization behavior makes NR unique among elastomers as far as strength properties are concerned. By blending SBR with NR, the mechanical property of the former could be improved. To the best of our knowledge, the transport behavior of SBR/NR blend membranes has not yet been examined. The important objective of the present study is a detailed investigation of the morphology, transport properties, and dynamic mechanical and mechanical behavior of SBR/NR blend membranes. Efforts have been made to correlate the transport behavior with the miscibility of the system and attempts have also been made to correlate the permeation and mechanical behaviors with the existing theoretical models.

EXPERIMENTAL

Materials

The SBR used was synaprene (1502) with a 25% styrene content (made by the emulsion process) supplied by Synthetic and Chemicals Ltd. (Bareilly, U. P., India. The NR used in this study was of ISNR-5 grade, supplied by the Rubber Research Institute of India (Kottayam). The solvents *n*-pentane, *n*-hexane, *n*-heptane, and *n*-octane (Merck India Ltd., Mumbai, India) were distilled twice before use. All other rubber ingredients were of laboratory reagent grade, supplied by Bayer India, Ltd. (Mumbai, India).

Table I Formulation of Mixes (in phr)

Ingredients	NR	SBR
Rubber	100	100
Zinc oxide	5	5
Stearic acid	1.5	2
MOR[a]	0.6	—
CBS[b]	—	1
TDQ[c]	1	1
Sulfur	2.5	2.2

phr, parts per hundred rubber.
[a] MOR, morpholine benzothiazyl sulphenamide.
[b] CBS-N, cyclohexyl-2-benzothiazyl sulphenamide.
[c] TDQ, trimethyl dihydroquinoline.

Preparation of SBR/NR Blends

The SBR/NR blends are denoted by N_0, N_{30}, N_{50}, N_{70}, and N_{100}, where the subscripts denote the weight percent of NR in them. The blends were prepared by blending the respective master batches on a two-roll mixing mill (friction ratio of 1:1.4), according to ASTM D15-627. The compounding recipe is given in Table I. The cure characteristics were studied in an elastograph (MDR-2000). The compounds were then compression-molded (along the mill grain direction using an electrically heated hydraulic press at 150°C for an optimum cure time t_{90} (Table II).

Morphology

Samples for the SEM studies were cryogenically fractured under liquid nitrogen. The NR phase was preferentially extracted from the cryogenically fractured samples by keeping the broken edge in petroleum ether for 72 h at room temperature. The NR-extracted samples were dried in an air oven. The samples were then sputter-coated with gold and the photographs were taken on a Phillip's model scanning electron microscope.

Swelling Experiments

Circular samples of diameter 1.9 cm were punched out from vulcanized sheets (dimension:15 $\times$ 15 $\times$ 2 cm^3) and immersed in solvents (15–20 mL) taken in test bottles kept at a constant temperature in an air oven. The samples were weighed at periodic intervals in an elec-

Table II Processing Characteristics

Blend Ratio	M_L (dN m)	M_H (dN m)	ts_1 (m : s)	ts_2 (m : s)	t_{90} (m : s)	CRI (min^{-1})
N_0 (SBR100)	1.13	7.13	7.48	8.48	17.02	11.71
N_{30} (SBR70/NR30)	0.79	7.23	5.59	6.53	13.09	15.24
N_{50} (SBR50/NR50)	0.65	6.72	4.59	5.54	11.40	17.06
N_{70} (SBR30/NR70)	0.53	6.09	4.06	5.05	10.23	19.30
N_{100} (NR100)	0.61	4.85	3.12	4.46	10.05	17.89

m : s, minute : second.

tronic balance (Sartorious, Italy) that measured reproducibly within ±0.001 g. The weighings were continued until equilibrium swelling was attained. A possible source of error in this method arises during the weighing operation where the sample has to be removed from the test bottle. However, since the weighing was done within 3040 s, the error could be neglected.[13] Similar methodology was adopted by several researchers.[14,15]

Dynamic Mechanical Testing

The dynamic mechanical properties of the blends were measured using a DMTA MKII (Polymer Laboratories). Compression-molded samples of dimensions 5 × 0.5 × 0.05 cm^3 were used for testing. The temperature range used was from −80 to +30°C and the frequencies ranged from 0.1 to 100 Hz.

Mechanical Testing

Mechanical testing was carried out using a universal testing machine (UTM) at 27°C with a crosshead speed of 50 mm/min using dumbbell-shaped tensile specimens according to ASTM D0412-80. These experiments were carried out for unswollen, swollen, and deswollen samples.

RESULTS AND DISCUSSION

Processing Characteristics

Elastographs of the mixes are given in Figure 1 and the processing characteristics are given in

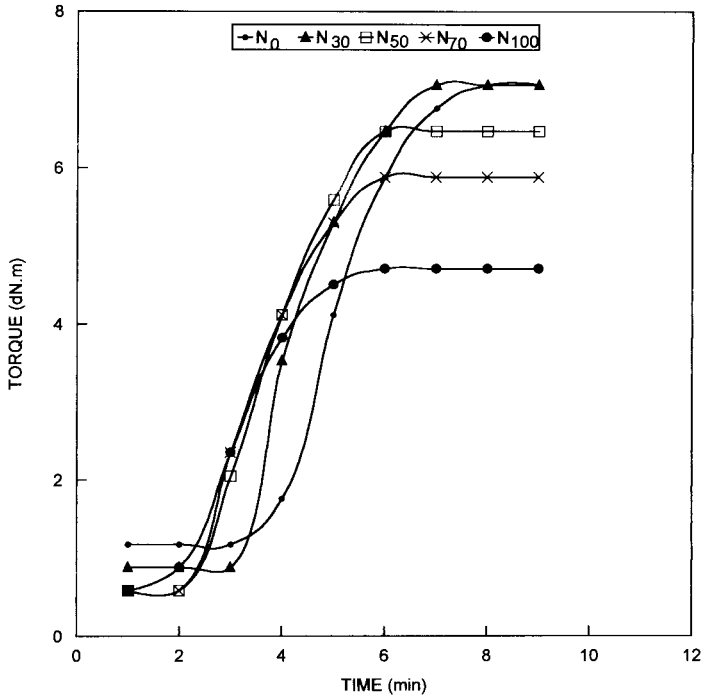

Figure 1 Elastographs of the mixes.

Table II. The minimum torque in the elastograph is presented as a minimum viscosity value (M_L) and is a measure of the extent of mastication. Minimum torque (M_L) values indicate that low viscosity is expected for the blend with the high NR content. The slight change in the M_L value in N_{100} might be due to the changes in the mixing time. The maximum torque in the elastograph (M_H) is an index of the crosslinking density and these values indicate that the maximum crosslinking density is possessed by N_0, and the minimum, by N_{100}. The blends possess intermediate values. The induction time (ts_1) is the time taken to start the vulcanization process. The ts_1 values decrease with increase in the NR content in the SBR/NR blend. N_{100} and N_{70} take the minimum time to initiate vulcanization among all the blend compositions. The scorch time (ts_2) is the time taken for the minimum torque value to increase by two units. It is a measure of the premature vulcanization of the material. The scorch time values in Table II indicate that pure SBR and SBR/NR blends with high SBR content exhibit better scorch safety. With increasing NR content in the blend, the scorch safety decreases. This behavior is associated with the high unsaturation of NR. The optimum cure time (t_{90}) is the vulcanization time to obtain optimum physical properties and is calculated using the equation

$$T_{90} = (M_H - M_L)0.9 + M_L \quad (1)$$

where T_{90} denotes 90% of the maximum torque. The time corresponding to T_{90} is the optimum cure time. The pure SBR compound shows a maximum optimum cure time. The t_{90} decreased with increase of the NR content in the blend. The cure rate index (CRI) is a direct measure of the fast curing nature of the rubber compounds and is calculated using the relation

$$\text{CRI} = 100/t_{90} - ts_2 \quad (2)$$

The CRI values are also given in Table II. SBR has the lowest CRI value and it increases with increase of the NR content in the blend composition. This trend is also associated with the high unsaturation of NR.

Morphology of Blends

The morphology of heterogeneous polymer blends depends on the blend composition, viscosity of the individual components, and processing history. Danesi and Porter[16] showed that for the same processing history the composition ratio and the melt viscosity differences for the components determine the morphology. Generally, for many blend systems, the least viscous phase was observed to form the continuous phase over a large composition range. The SEM photographs presented in Figure 2 show the morphology of the SBR/NR blends. Figure 2(a) shows the morphology of the N_{30} blend, in which NR is dispersed as domains in the continuous SBR matrix. The average domain size of the dispersed particles is 3.2 μm. The two-phase morphology significantly influences the permeation properties. Figure 2(b,c) represents the morphology of the N_{50} and N_{70} blends. In Figure 2(b,c), NR becomes continuous and the system exhibits a cocontinuous morphology. Morphology studies revealed that SBR/NR blends are heterogeneous in nature.

Dynamic Mechanical Analysis

The dynamic mechanical properties such as storage modulus (E'), loss modulus (E''), and damping (tan δ) of SBR, NR, and their blends were evaluated from -80 to 30°C. A dynamic mechanical investigation was used to predict the miscibility of the system by various researchers. Generally, for an incompatible blend, the tan δ versus temperature curve shows the presence of two tan δ or damping peaks corresponding to the glass transition temperatures of individual polymers. For a highly compatible blend, the curve shows only a single peak in between the transition temperatures of the component polymers, whereas broadening of the transition occurs in the case of a partially compatible system. In the case of compatible and partially compatible blends, the T_g's are shifted to higher or lower temperatures as a function of the composition. The variation of tan δ with temperatures of the SBR, NR, and SBR/NR blends is shown in Figure 3. The tan δ curve of NR shows a peak at -51°C due to the α-transition arising from the segmental motion. This corresponds to the glass transaction temperature (T_g) of NR. SBR shows the glass transition temperature at 39°C in the tan δ versus temperature curve. NR has higher damping than that of SBR. The blends show two tan δ peaks around -54 and -35°C, which correspond to the T_g's of NR and SBR, respectively. The two separate peaks corresponding to the T_g's of NR and SBR indicate that the blends are not compatible.

The variation of tan δ_{max} as a function of the NR content is shown in Figure 4. It can be seen that the tan δ_{max} value due to the NR phase

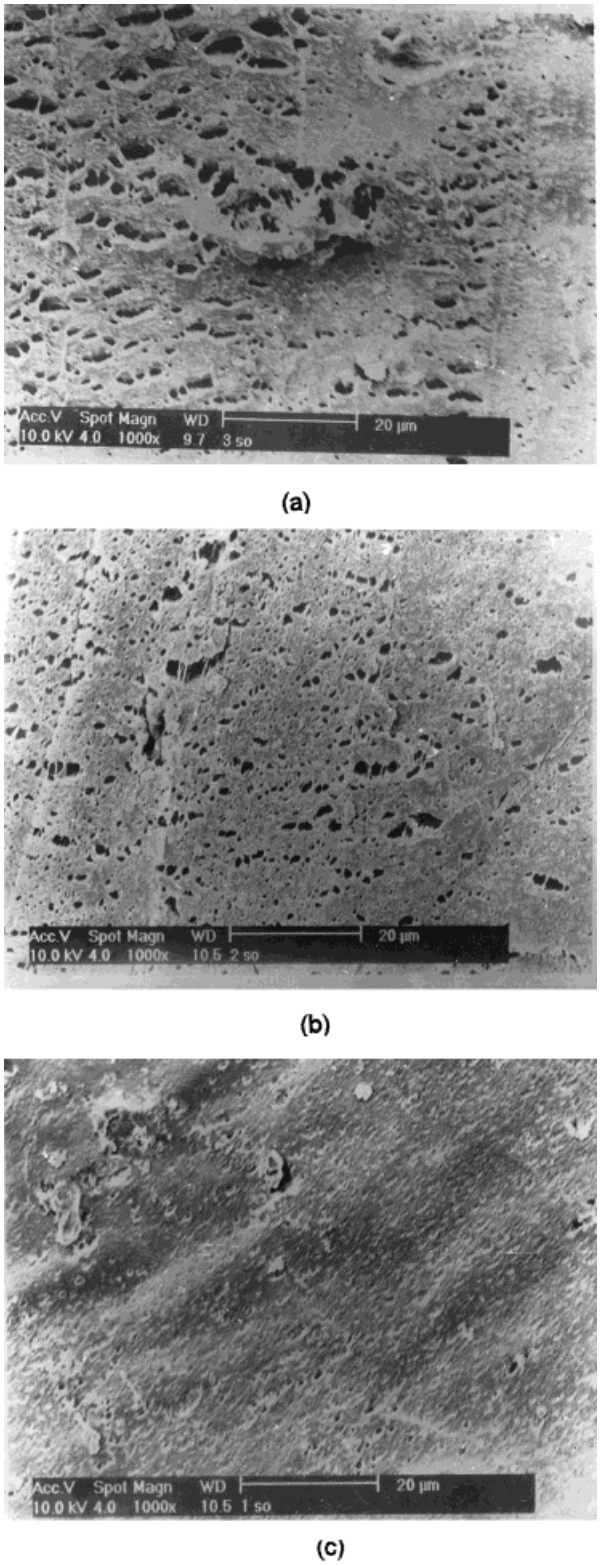

Figure 2 SEM photographs of the morphology of the blends: (a) N_{30}; (b) N_{50}; (c) N_{70}.

increases as the SBR content decreases, that is, the damping increases as the NR content increases. The damping due to the SBR phase decreases because of the lower concentration of the SBR phase. The variation in tan δ_{max} can be related to the morphology of the blend. The tan δ_{max} due to the NR phase increases sharply after 50% because of the higher contribution of tan δ_{max} from the continuous NR phase. But tan δ_{max} of SBR decreases as the NR content increases and the decrease is much sharper when the NR content is 50% or more, where NR forms a continuous phase. The variation of the storage modulus, E', of the blends as a function of temperature is shown in Figure 5. All curves show three distinct regions, that is, glassy, transition, and rubbery regions. The temperature region between -70 and -58°C is the glassy region and between -57 and -41°C is the transition region. There is a wide rubbery region, that is, from -40 to 19°C.

The storage modulus is found decrease with increase in the temperature due to the decrease in stiffness of the sample. At the low-temperature region, N_{100} exhibits the highest modulus, and N_0, the lowest. At the high-temperature region, N_{50} has the maximum modulus and N_{30} has the minimum one.

The variation of the loss modulus (E'') with temperature (Fig. 6) also shows the same trend as that of tan δ, that is, the curves show a maximum corresponding to the glass transition temperature of NR and SBR. The loss modulus decreases with increase in the NR content. Thus, dynamic mechanical analysis established the two-phase structure of the SBR/NR blends.

The influence of the frequency on the storage modulus, loss modulus, and tan δ of the N_{50} sample is shown in Figures 7, 8, and 9, respectively. The storage modulus increased with increasing frequency from 0.1 to 50 Hz, whereas it decreased with increasing temperature (Fig. 7). The loss modulus decreased initially with increase of the frequency, and after passing through the transition region, an increase was observed. At the low-temperature region, the tan δ values decreased with increase of the frequency and just the reverse occurred at the high-temperature region. It was also found that the tan δ_{max} shifts to the high-temperature region at higher frequencies.

Three-dimensional graphs showing the variation of tan δ with the frequency and temperature of N_0 are given in Figure 10. It is very clear that the transition temperature shifts to the higher-temperature side with increasing frequency. In the case of blends, two well-defined transitions

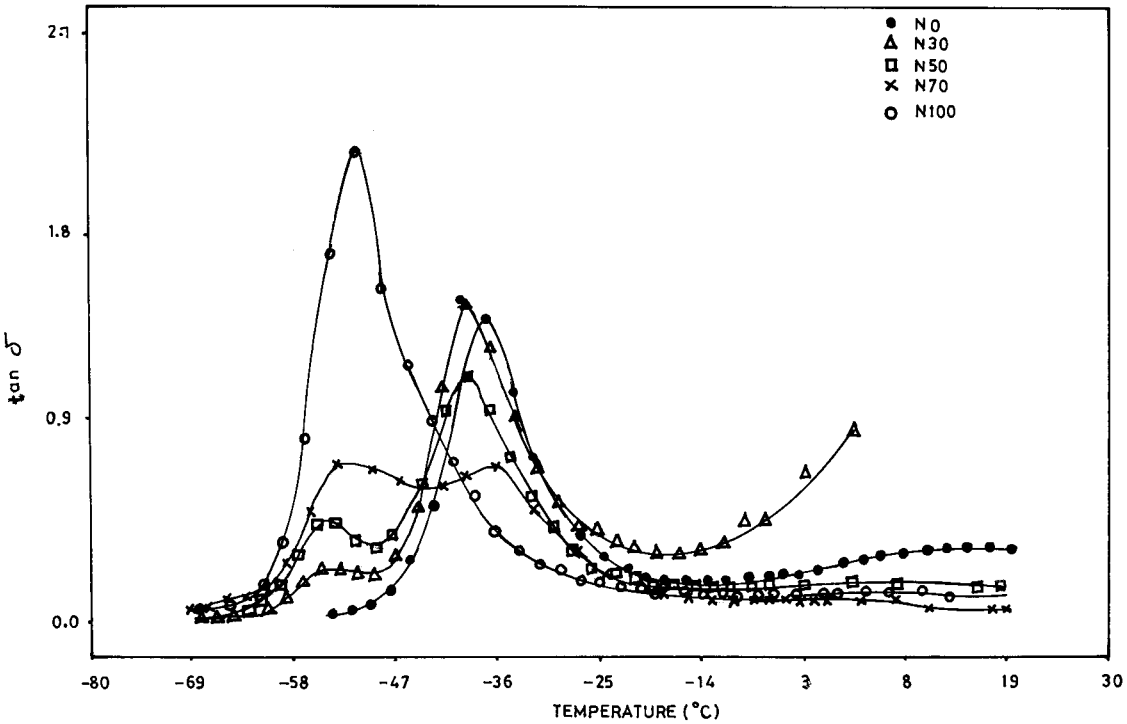

Figure 3 Variation of tan δ with temperature of SBR/NR blends.

could be seen in the three-dimensional plot. Figure 11 shows the Cole–Cole plot of the N_{50} blend where the loss modulus (E'') data are plotted as a function of the storage modulus (E'). It is also reported that a homogeneous polymeric system shows a semicircle diagram, while heterophase systems show two modified semicircles.[17] In this case, the blends show a behavior different from that of the homogeneous system, due to the presence of two components which are immiscible.

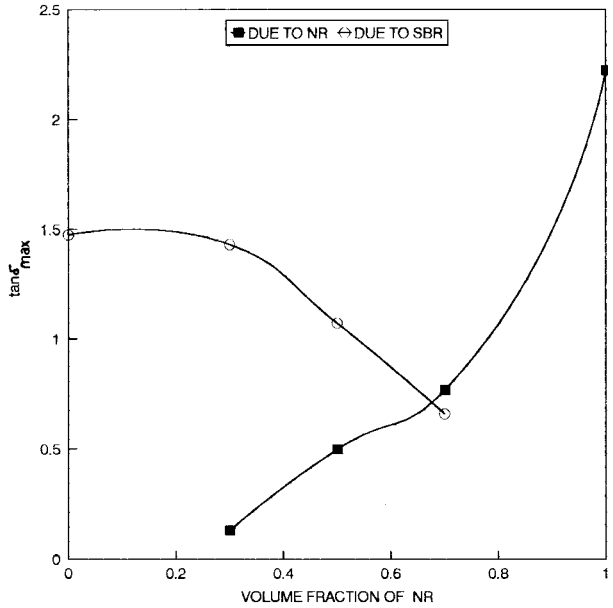

Figure 4 Variation of tan δ_{max} as a function of NR content.

Mechanical Properties

The stress–strain curves of the unswollen, swollen, and deswollen samples are illustrated in Figures 12, 13, and 14, respectively. The nature of the deformation of the blends under an applied load can be understood from the stress–strain curves. The deformation curves of the homopolymers and their blends are similar. It can be understood from Figure 12 that at a low strain level N_0 has the maximum stress and N_{100} has the minimum. The blend compositions have intermediate values. The stress required to break the sample increased with increase in the NR content. This is due mainly to the strain-induced crystallization behavior of NR.

The stress–strain curves of the samples after reaching equilibrium saturation in *n*-hexane reveal that there is some difference in the nature of the stress–strain behavior after reaching equilibrium. The stress at low strain level (<100%) follows the same pattern as that in the case of the unswollen samples. With increasing NR content,

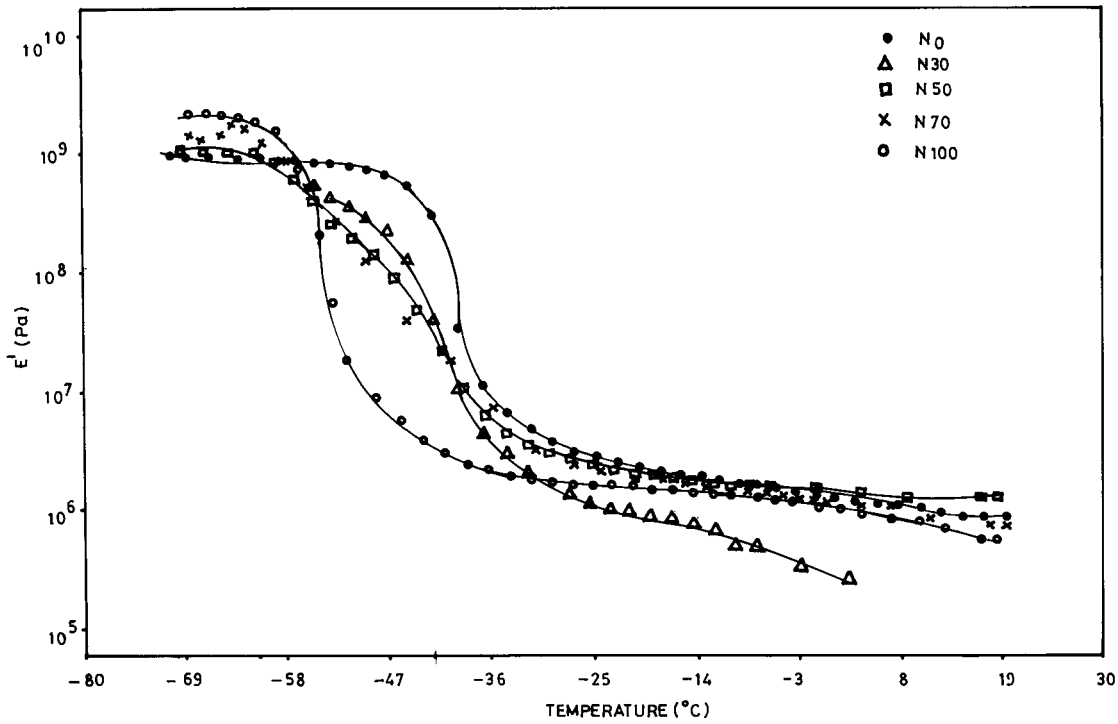

Figure 5 Variation of storage modulus (E') of SBR/NR blends as a function of temperature.

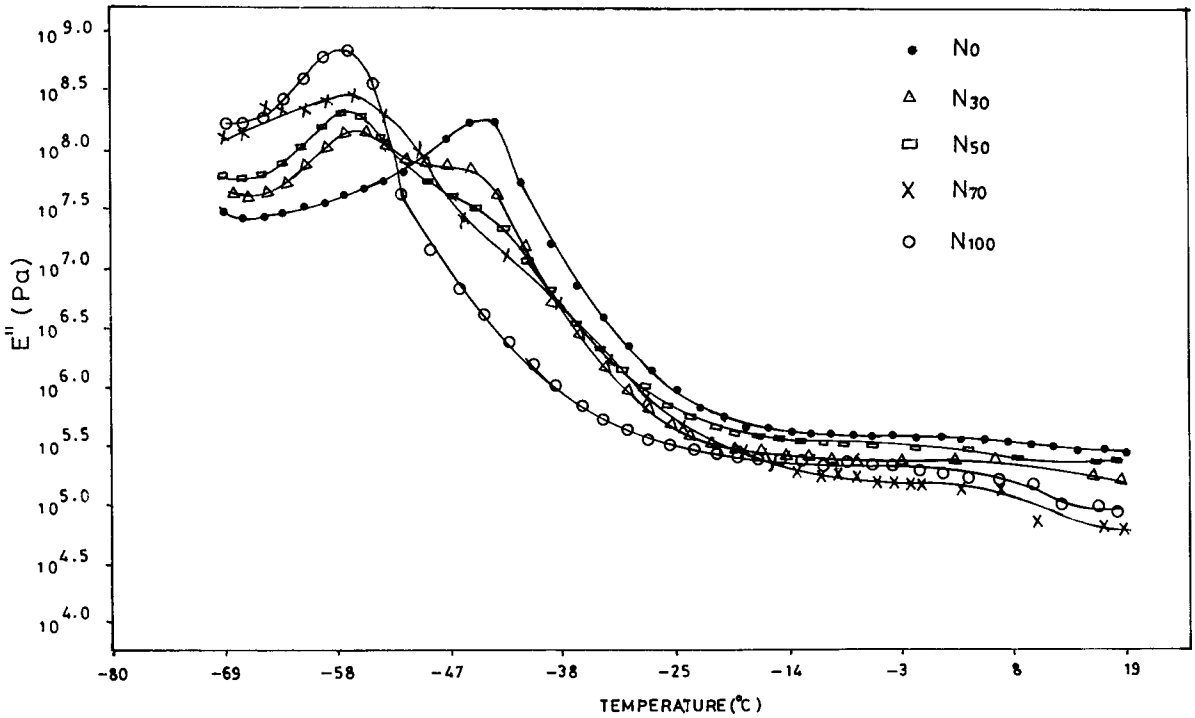

Figure 6 Variation of loss modulus as (E'') of SBR/NR blends as a function of temperature.

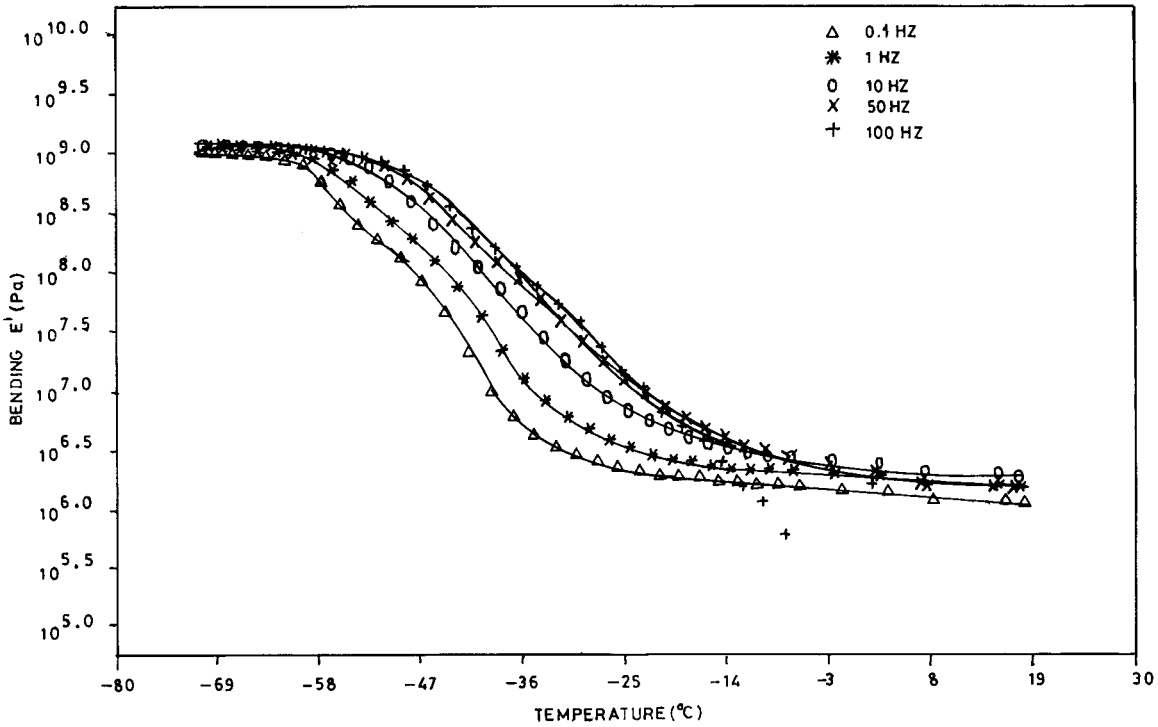

Figure 7 Variation of storage modulus (E') of N_{50} sample as a function of frequency.

the stress–strain curve loses its typical elastomeric behavior. It was also found that the maximum stress increases with increase of the NR content up to 50% and then decreases. This is the result of the lack of strain-induced crystallization behavior in the swollen samples, particularly

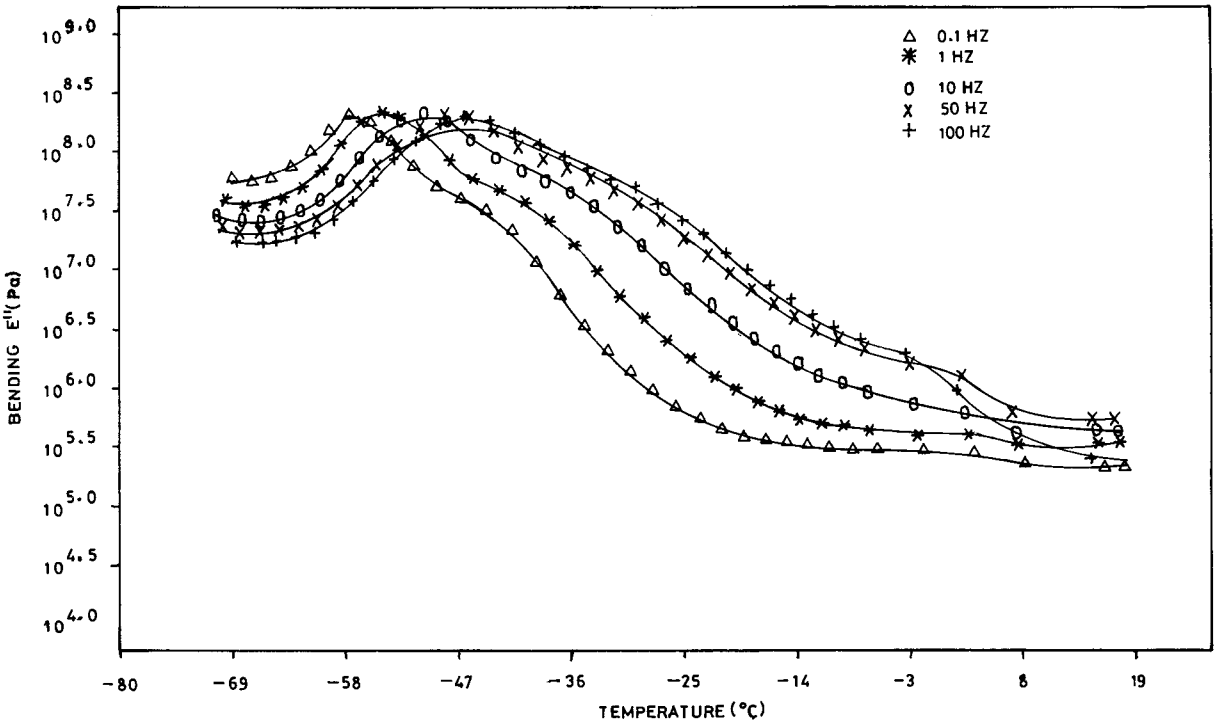

Figure 8 Variation of loss modulus of (E'') N_{50} sample as a function of frequency.

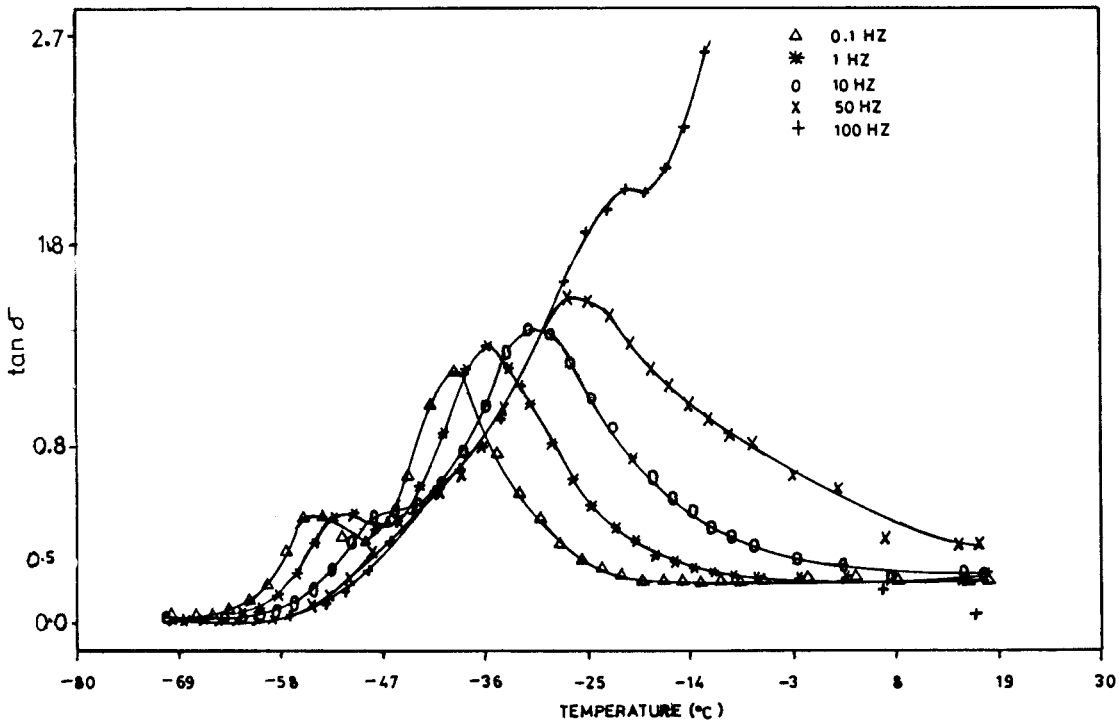

Figure 9 Variation of tan δ of N_{50} sample as a function of frequency.

samples with high NR content. The presence of solvents in the swollen samples restricts the mobility of the polymeric chains and therefore the orientation is difficult. The stress–strain behavior of the deswollen samples is similar to those of the unswollen samples. But there is an overall increase in the magnitude of the maximum stress value. This increase in properties is attributed mainly to the increased interchain interaction after the sorption–desorption process.

The mechanical properties of homopolymers and blends are given in Table III. The properties such as tensile strength and elongation at break were increased from N_0 to N_{100}. The mechanical strength of SBR increases upon blending it with NR. This is definitely associated with the strain-

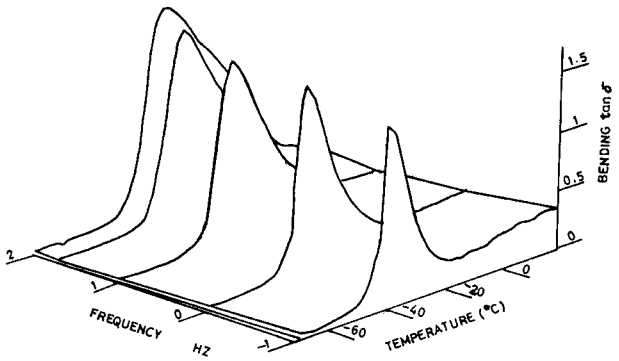

Figure 10 Variation of tan δ with frequency for N_0 sample.

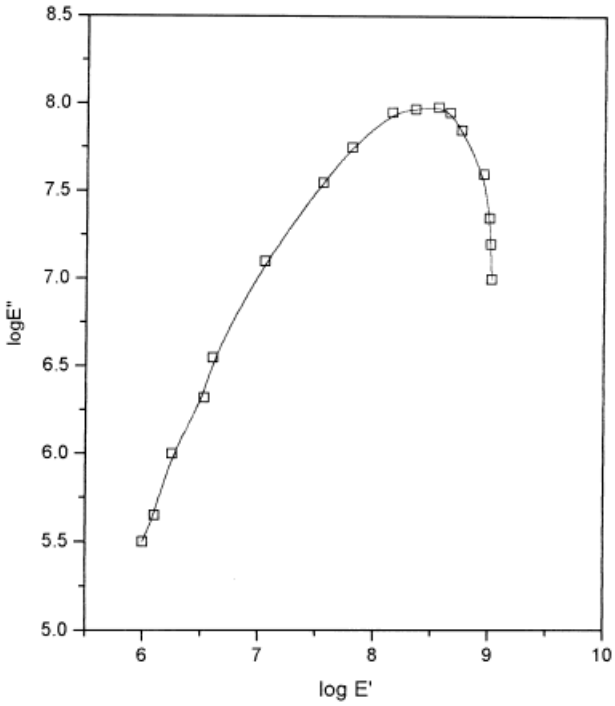

Figure 11 Cole–Cole plot of N_{50} sample.

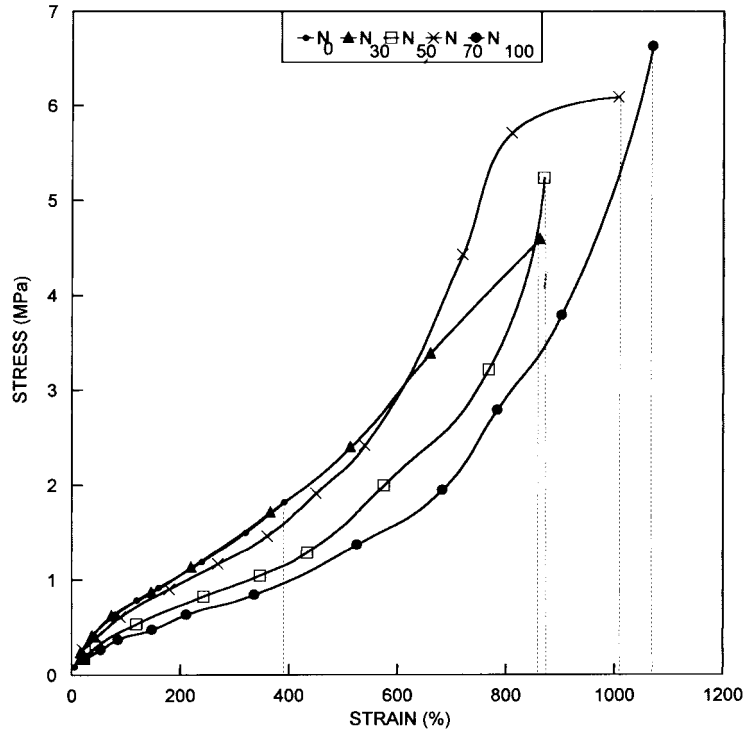

Figure 12 Stress–strain curves of unswollen SBR/ NR blends.

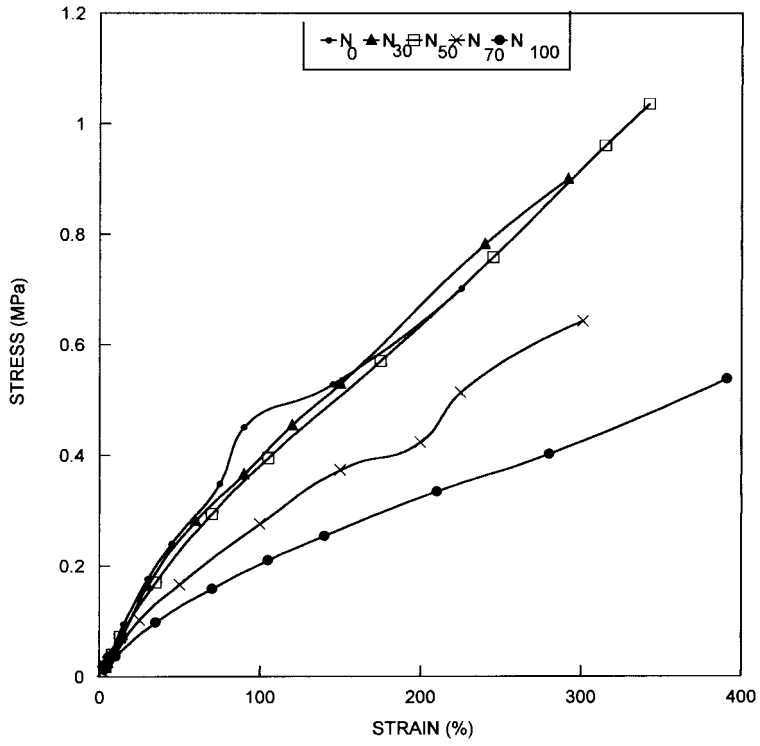

Figure 13 Stress–strain curves of swollen SBR/NR blends in *n*-hexane.

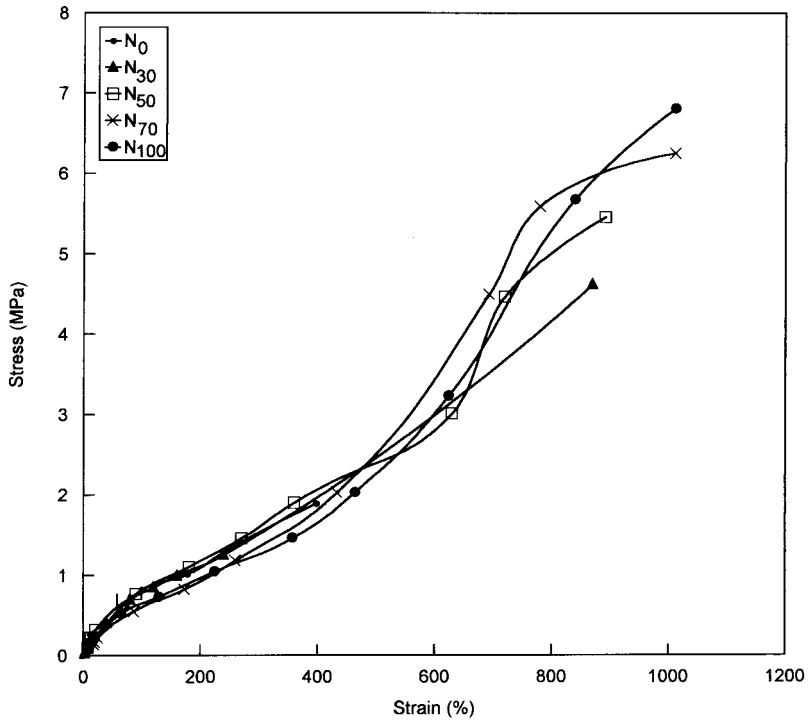

Figure 14 Stress–strain curves of deswollen SBR/NR blends.

induced crystallization of NR. The Young's modulus decreased from N_0 to N_{100}, which indicates that the initial stretching of SBR and the blend with the higher SBR content requires higher stress. In the swollen state, there is overall reduction in the magnitude of all the mechanical properties. The tensile behavior of the swollen specimens are governed by two types of relaxation mechanisms: the intramolecular motions of segments and the molecular motions involving the adjustments and shifting of chain entanglements. In the equilibrium swollen state, the rubber–sol-

Table III Mechanical Properties of SBR/NR Blends

Sample	System	Tensile Strength (MPa)	Elongation at Break (%)	Young's Modulus (MPa)	Secant Modulus (MPa)		
					M_{100}	M_{200}	M_{300}
Unswollen	N_0	1.82	391	1.36	0.43	1.05	1.24
	N_{30}	4.59	862	1.22	0.62	1.01	1.35
	N_{50}	5.24	869	0.80	0.66	0.98	1.34
	N_{70}	6.09	1007	0.62	0.64	0.96	1.27
	N_{100}	6.63	1069	0.35	0.37	0.58	0.79
Swollen	N_0	0.70	225	0.68	0.43		
	N_{30}	0.90	291	0.49	0.38	0.66	
	N_{50}	1.04	342	0.59	0.36	0.63	0.90
	N_{70}	0.64	362	0.43	0.27	0.42	
	N_{100}	0.54	390	0.32	0.20	0.32	0.42
Deswollen	N_0	1.89	398	1.72	0.883		
	N_{30}	4.62	870	1.545	0.749	1.119	1.524
	N_{50}	5.40	892	1.69	0.814	1.159	1.60
	N_{70}	6.25	1012	0.603	0.959	1.343	
	N_{100}	6.81	1080	0.976	0.625	1.04	1.40

vent interaction is maximum and the rubber–rubber interaction is minimum. This gives rise to the abrupt decrease of the tensile properties of the swollen samples. The mechanical properties of the deswollen samples showed an improvement compared to the unswollen samples. This might be due to increase in the interchain interaction after a sorption–desorption process.

Model Fitting

The mechanical behavior of the blends was modeled using various composite models such as the parallel, the series, the Kerner, and the Kunori models. The parallel model (highest upper-bound model) is given by the equation[18]

$$M = M_1\phi_1 + M_2\phi_2 \tag{3}$$

where M is the mechanical property of the blend and M_1 and M_2 are the mechanical properties of components 1 and 2, respectively, and ϕ_1 and ϕ_2 are the volume fractions of components 1 and 2, respectively. The lowest lower-bound series model is found in models in which the components are arranged in series with the applied stress. The equation for this case is[18]

$$1/M = \phi_1/M_1 + \phi_2/M_2 \tag{4}$$

Kunori and Geil[19] reported that when a strong adhesive force exists between the blend components the dispersed phase will contribute to the strength of the blend and the equation is

$$\sigma_b = \sigma_m(1 - A_d) + \sigma_d A_d \tag{5}$$

where A_d represents the area occupied by the dispersed phase in the transverse cross section.

Considering two possible fracture paths in a blend, the equation can be modified as follows depending on whether the fracture is through the interface or through the matrix: When the fracture is through the interface,

$$\sigma_b = \sigma_m(1 - \phi_d^{2/3}) + \sigma_d\phi_d^{2/3} \tag{6}$$

when the fracture is through the matrix,

$$\sigma_b = \sigma_m(1 - \phi_d) + \sigma_d\phi_d \tag{7}$$

where σ_b, σ_m, and σ_d are the properties of the blend, matrix phase, and dispersed phase, respectively, and ϕ_d is the volume fraction of the dispersed phase. Another important model for perfect adhesion is the Kerner equation.[20] According to this,

$$E = E_c \frac{\begin{array}{l}\phi_d E_d/(7 - 5\nu_m)E_m \\ \quad + (8 - 10\nu_m)E_d + \phi_m/15(1 - \nu_m)\end{array}}{\begin{array}{l}\phi_d E_m/(7 - 5\nu_m)E_m \\ \quad + (8 - 10\nu_m)E_d + \phi_m/15(1 - \nu_m)\end{array}} \tag{8}$$

where E, E_m, and E_d are the respective properties of the blend, continuous phase, and dispersed phase; ϕ_d and ϕ_m, the volume fractions of the dispersed and continuous phases; and ν_m, the Poisson's ratio of the continuous phase.

Figure 15 shows the theoretical and experimental curves of the tensile strength values of the SBR/NR blend. In N_{30} and N_{50}, the experimental values are close to that of the Kunori model. Therefore, it can be concluded that the fracture propagates through the interface rather than through the matrix. But in N_{70}, the experimental value is close to that of parallel model, Therefore, in N_{70}, it can be concluded that the applied stress distributes equally in two phases.

Transport Properties: Effect of Blend Composition

The sorption behavior of SBR/NR blends in hexane is displayed in Figure 16. The SBR, NR, and NR/SBR blends show almost a similar sorption behavior even though the corresponding maximum uptake is different. The initial portions of the sorption curves are sigmoidal in shape. According to Southern and Thomas,[21] when a polymer interacts with solvents, the surface of the polymer sample immediately swells, but the swelling is prevented by the underlying unswollen material. Thus, a two-dimensional compression stress is produced in the surface. The swelling stresses are either relaxed or dissipated by further swelling and rearrangement of the segments. The sigmoidal nature is associated with the time taken by the polymer segments to respond to the swelling stresses and to rearrange themselves to accommodate the penetrant molecule. N_{100} shows the maximum solvent uptake, and N_0, the minimum. The maximum solvent uptake increases with increase in the volume fraction of NR. It is established that the permeability of heterogeneous rubber–rubber blends is intermediate between that of the components.[22] The observed solvent uptake is in accordance with this observation. The morphology of the blends also contributes toward the transport behavior. The two-phase morphology of the N_{30} blend [Fig. 2(a)]

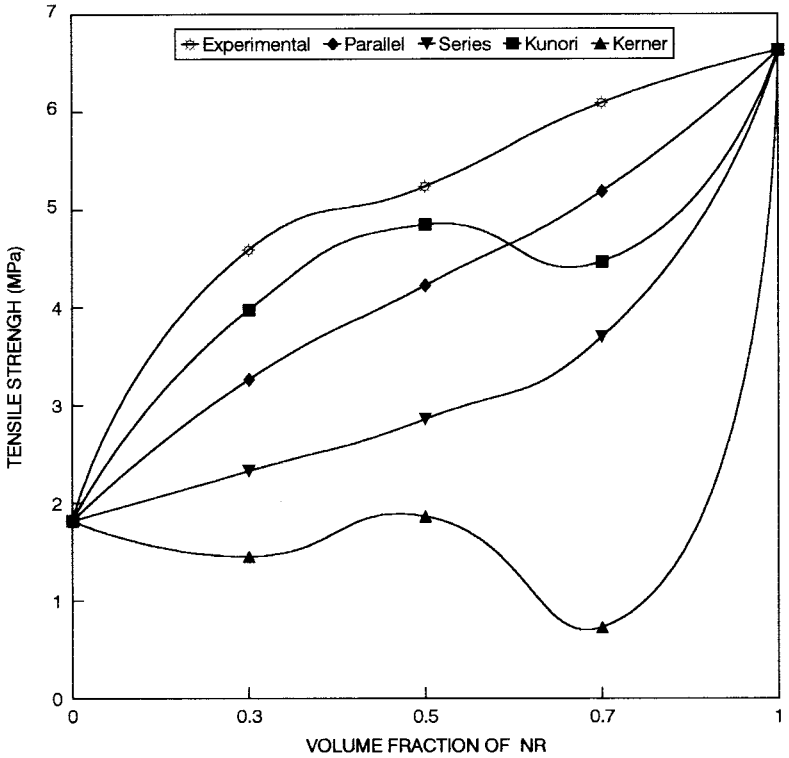

Figure 15 Comparison of experimental tensile strength with theoretical values as a function of volume fraction of NR.

makes a tortuous path for the penetrant and, hence, the net uptake is low. Due to the cocontinuous morphology of the N_{50} and N_{70} blends [Fig. 2(b,c)], the passage of the penetrant becomes easier and, hence, the uptake is high. With increasing volume fraction of NR in the blend, the chain flexibility increases due to the low glass transition temperature of NR (T_g of NR −51°C and that of SBR −39°C) and, hence, the solvent uptake.

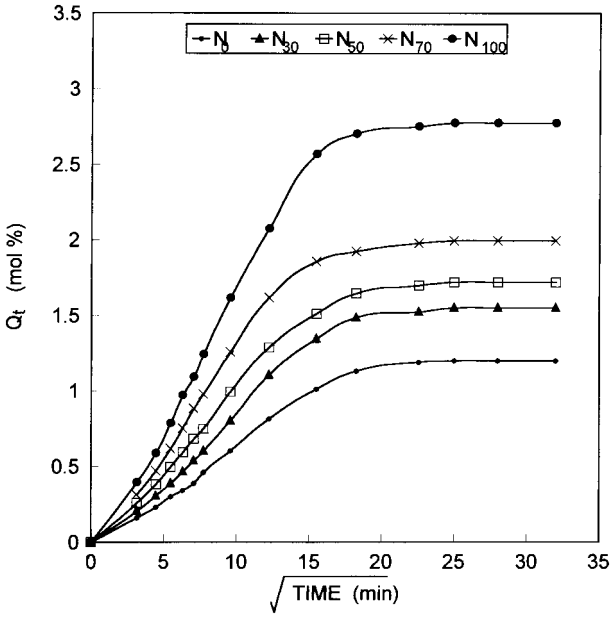

Figure 16 Mol percent hexane uptake of SBR/NR blends.

To further establish the sorption behavior, we calculated the molar mass between the crosslinks (M_c) using the Flory–Rehner relation[23]:

$$M_c = \frac{-\rho_p V_s V_r^{1/3}}{[\ln(1 - V_r) + V_r + \chi V_r^2]} \quad (9)$$

where ρ_p is the density of the polymer; V_s, the molar volume of the solvent; V_r, the volume fraction of the polymer in the swollen sample; and χ, the Flory–Rehner interaction parameter. The degree of crosslinking (n_1) can be estimated from the M_c values using the following equation:

$$n_1 = 1/2M_c \quad (10)$$

The n_1 values are 1.98×10^{-4}, 1.33×10^{-4}, 1.25×10^{-4}, 1.09×10^{-4}, and 0.743×10^4 mol/cc, respectively, for N_0, N_{30}, N_{50}, N_{70}, and N_{100}. As

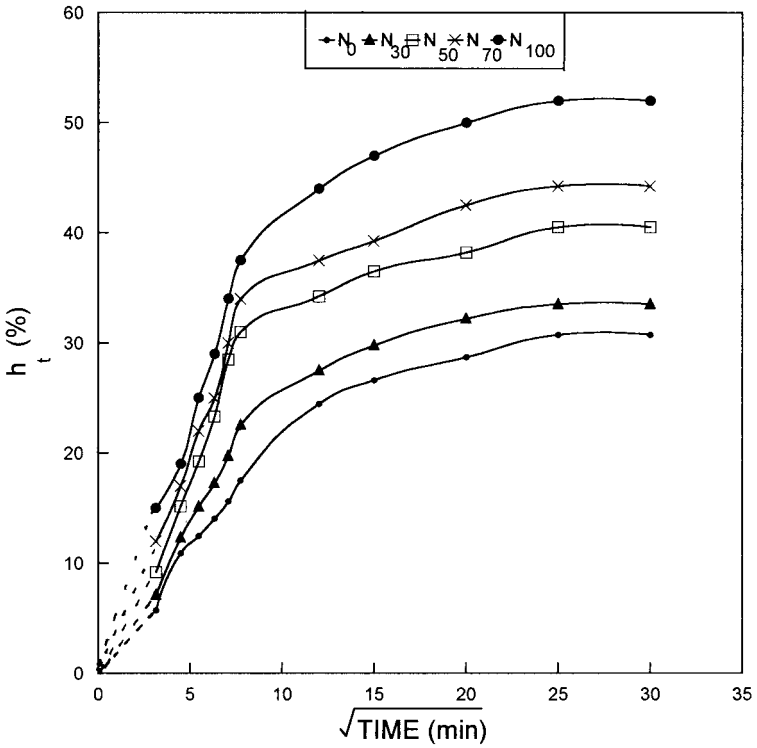

Figure 17 Variation of change in thickness (*ht %*) with square root of time.

the degree of crosslinking increases, the swelling decreases. From N_0 to N_{100}, the degree of crosslinking decreases and, hence, the observed sorption behavior. The thickness of the sample was monitored to understand the variation of the swelling in the thickness direction.[24] The resulting plots are shown in Figure 17. It is revealed from the figure that the variation in thickness has the same order as that of the swelling, that is, h_t % increase in the order $N_0 < N_{30} < N_{50} < N_{70} < N_{100}$.

The influence of the penetrant size on the sorption behavior of the N_{50} blend is shown in Figure 18. The maximum solvent uptake increases with increasing penetrant size from pentane to heptane and decreases for octane. This behavior can be explained based on the solubility parameter difference between the polymer and the penetrant. Froething et al.[25] and Lee et al.[26] reported that the differences in the solubility parameter between the polymer and the penetrant has a role in deciding the sorption behavior of the penetrant in the polymer membrane. It is found that as the solubility parameter for the polymer and solvent becomes close to one another the solubility of the latter in the polymer becomes high. Figure 19 shows the variation of the maximum solvent uptake with the solubility parameter difference between the polymer and the solvent. Alhough this value is the lowest for octane, the lowest solvent uptake for octane is due to its larger size and increased number of conformations compared to pentane, hexane, and heptane. But for the other three solvents, the uptake is in accordance with the solubility parameter difference.

Diffusivity, Sorptivity, and Permeability

The diffusivity was calculated using the relation[27]

$$\frac{Q_t}{Q_\infty} = \sum_{n=0}^{n=\infty} 8/(2n+1)^2\pi^2 e - \{(2n+1)^2\pi^2 Dt/h^2\} \tag{11}$$

where t is the time; h, the initial sample thickness; and D, the diffusion coefficient or diffusivity. This equation can be readily solved, but it is instructive to examine the short-time limiting expression as well:

$$\frac{Q_t}{Q_\infty} = \frac{[4]}{\pi^2}\frac{[Dt]^{1/2}}{h^2} \tag{12}$$

A single master curve is obtained from a plot of Q_t versus $t^{1/2}$, which is initially linear. Thus, D can be calculated from a rearrangement of eq. (6) as[28]

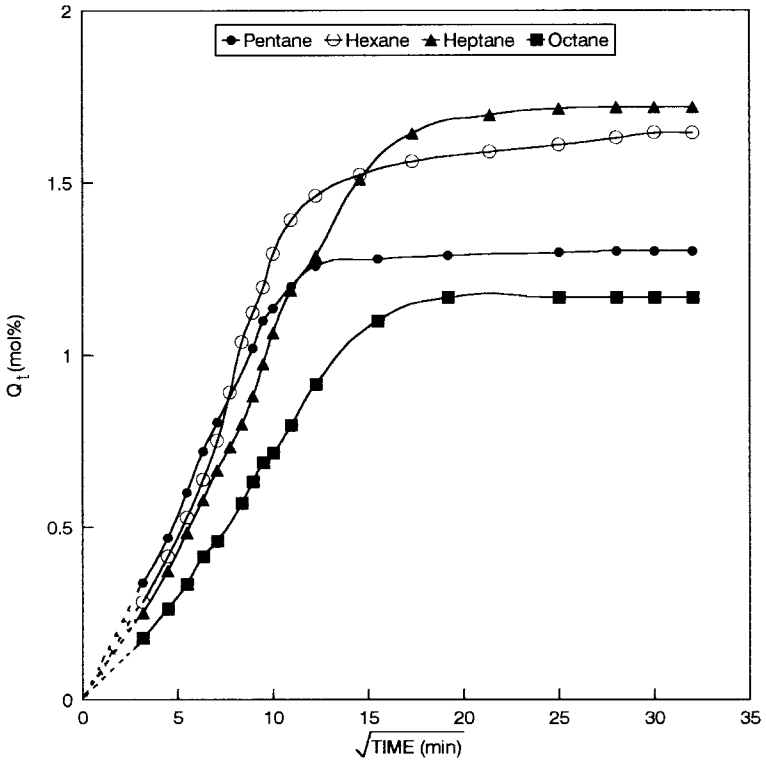

Figure 18 Mol percent uptake of N_{50} in *n*-alkanes.

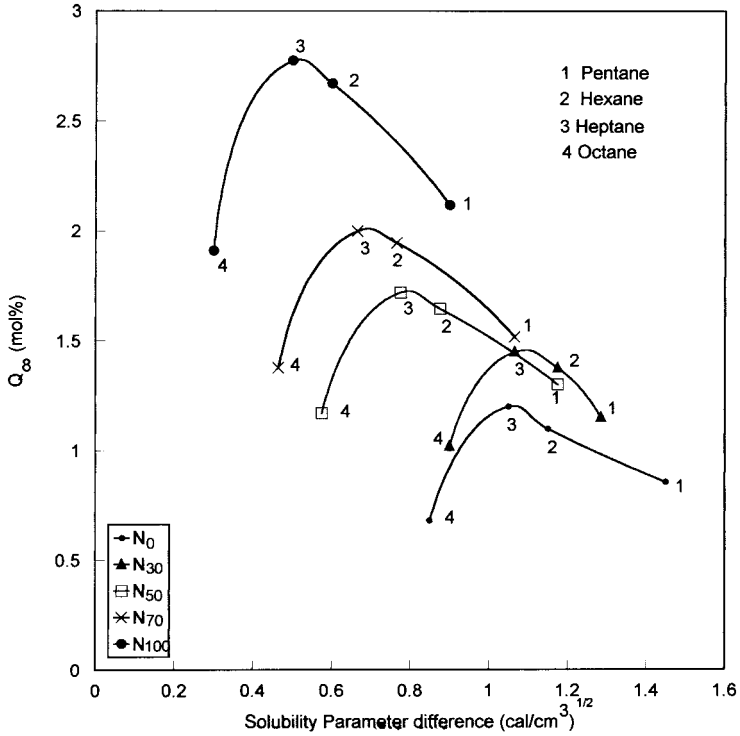

Figure 19 Variation of maximum solvent uptake with solubility parameter difference between polymer and solvent.

Table IV Diffusivity ($D^* \times 10^5$) cm²/s

Solvent	Temperature (°C)	N_0	N_{30}	N_{50}	N_{70}	N_{100}
Pentane	25	0.472	0.622	0.882	1.10	1.82
Hexane	25	0.595	0.620	0.802	0.926	1.75
	40	0.703	0.919	1.08	1.09	2.74
	50	0.749	1.276	1.36	1.94	3.30
	60	0.763	1.32	1.56	2.14	3.56
Heptane	25	0.435	0.550	0.758	1.156	1.57
	40	0.495	0.593	0.817	1.267	1.83
	50	0.583	0.675	0.813	1.20	1.93
	60	0.971	0.877	1.08	1.40	2.58
Octane	25	0.313	0.43	0.652	0.848	1.25
	40	0.338	0.595	0.618	1.012	1.45
	50	0.520	0.740	1.014	1.30	1.96
	60	0.772	0.910	1.30	1.66	2.32

$$D = \pi(h\theta/4Q_\infty)^2 \quad (13)$$

where θ is the slope of the linear portion of the sorption curve Q_t versus $t^{1/2}$. Because significant swelling of the samples was observed during the sorption experiments in all the solvents, a correction to the diffusion coefficient under the swollen condition was essential. This was done by calculating the intrinsic diffusion coefficient (D^*) from the volume fraction of the swollen rubber by using the following relation[29]:

$$D^* = D/(V_r)^{7/3} \quad (14)$$

The calculated values of D^* are given in Table IV. The D^* values of the blends are found to be intermediate between those of the components. The variation of the D^* value with the volume fraction of NR is given in Figure 20.

The sorption coefficient (S) is a thermodynamic parameter, which depends on the strength of the interactions in the polymer/penetrant mixture. It is calculated from the equilibrium swelling using the equation[28]

$$S = M_\infty/M_0 \quad (15)$$

where M_∞ is the mass of the solvent at swelling equilibrium and M_0 is the mass of the dry polymer. The computed S values are given in Table V. Just like D^*, the S values of the blends are also intermediate between those of individual components. The S values are highest in heptane due to its closer solubility parameter with the polymer.

Permeability is a combination of sorption and diffusion processes. Hence, P can be determined from the following empirical relation[28]:

$$P = D^*S \quad (16)$$

The estimated P values are given in Table VI. The P values decrease gradually from hexane to octane. The P values are comparably low in pentane due to the low sorption coefficient. There is a sharp increase in the values of D^*, S, and P after

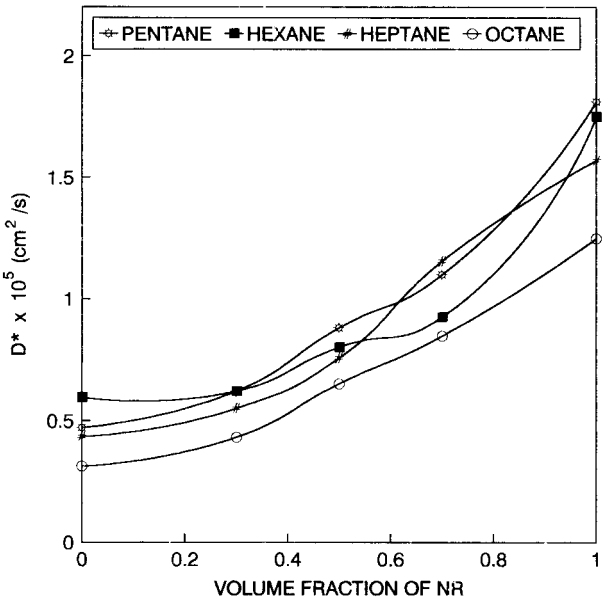

Figure 20 Variation of diffusion coefficient with volume fraction of NR.

Table V Sorptivity *S* (g/g)

Solvent	Temperature (°C)	N_0	N_{30}	N_{50}	N_{70}	N_{100}
Pentane	25	0.618	0.801	0.939	1.09	1.53
Hexane	25	0.925	1.157	1.38	1.636	2.246
	40	0.965	1.164	1.403	1.606	2.16
	50	1.004	1.202	1.38	1.543	2.17
	60	1.04	1.18	1.35	1.62	2.18
Heptane	25	1.201	1.44	1.722	2.00	2.78
	40	1.248	1.49	1.725	1.925	2.62
	50	1.282	1.526	1.706	1.87	2.68
	60	1.285	1.505	1.693	1.984	2.71
Octane	25	0.775	1.165	1.334	1.57	2.17
	40	0.954	1.186	1.452	1.52	2.09
	50	1.053	1.237	1.417	1.51	2.12
	60	1.09	1.225	1.407	1.56	2.14

30 wt % of NR. The increase in the values of P is much sharper in N_{50} and N_{70} due to its co-continuous nature.

Composite models such as parallel, series, Maxwell, and Robeson models were applied to the SBR/NR system to predict the permeability properties of these blends. In the parallel model, the highest bound permeability is given by the equation[1]

$$P = P_1\phi_1 + P_2\phi_2 \tag{17}$$

where P is the permeability of the blend; P_1 and P_2, the permeabilities of components 1 and 2, respectively; and ϕ_1 and ϕ_2, the volume fractions of components 1 and 2, respectively. The parallel model is applicable to systems in which the components are arranged parallel to one another. The lowest-bound series model is found in models in which the components are arranged in series. The equation for this case is[1]

$$1/P = \phi_1/P_1 + \phi_2/P_2 \tag{18}$$

According to the Maxwell equation,[1]

$$P = P_m[P_d + 2P_m - 2\phi_d(P_m - P_d)/ P_d + 2P_m + \phi_d(P_m - P_d)] \tag{19}$$

Table VI. Permeability P^* ($= D^*S$) $\times 10^5$ cm^2/s

Solvent	Temperature (°C)	N_0	N_{30}	N_{50}	N_{70}	N_{100}
n-Pentane	25	0.292	0.498	0.828	1.199	2.70
n-Hexane	25	0.554	0.719	1.11	1.516	6.16
	40	0.778	1.07	1.48	1.76	7.16
	50	0.752	1.58	1.87	2.99	7.16
	60	0.793	1.56	2.09	3.47	7.77
n-Heptane	25	0.523	0.792	1.31	2.32	4.36
	40	0.617	0.88	1.410	2.44	4.78
	50	0.75	0.984	1.39	2.26	5.13
	60	1.25	1.32	1.83	2.79	6.97
n-Octane	25	0.243	0.504	0.870	1.313	2.72
	40	0.322	0.705	0.898	1.54	3.02
	50	0.546	0.915	1.44	1.97	4.15
	60	0.841	1.157	1.83	2.53	4.95

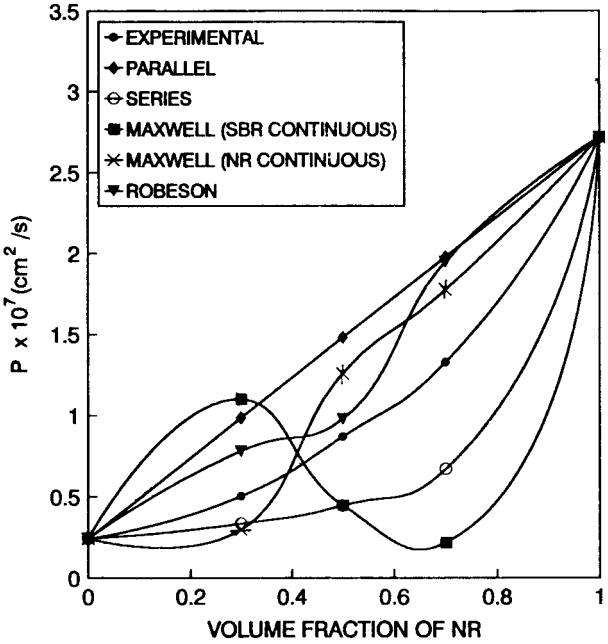

Figure 21 Comparison of experimental permeability with theoretical predictions.

where the subscripts m and d refer to the continuous matrix phase and the dispersed phase, respectively. Robeson extended Maxwell's analysis by assuming that at intermediate concentrations both phases contribute continuous and discontinuous characteristics. The resulting Robeson equation is[1]

$$P = X_a P_1 \frac{[P_2 + 2P_1 - 2\phi_2(P_1 - P_2)]}{[P_2 + 2P_1 + \phi_2(P_1 - P_2)]} + X_b P_2 \frac{[P_1 + 2P_2 - 2\phi_1(P_2 - P_1)]}{[P_1 + 2P_2 + \phi_1(P_2 - P_1)]} \quad (20)$$

where X_a represents the fraction of the composition in which component 1 is the continuous phase and X_b corresponds to a continuous phase of component 2. The description of such a cocontinuity is limited by the restriction that

$$X_a + X_b = 1 \quad (21)$$

Figure 21 shows the experimental and theoretical curves of permeability as a function of the volume fraction of NR. It can be seen from the figure that the experimental data at different volume fractions of NR (say 0.3, 0.5, and 0.7) are close to the series model, Robeson model, and Maxwell (NR continuous) model, respectively.

Interaction Parameter

The interaction parameter (χ), signifying the interaction between the polymer blend and the permeant, is determined using the relation[30]

$$\chi = \beta + V_s/RT(\delta_s - \delta_p)^2 \quad (22)$$

where β is the lattice constant; V_s, the molar volume of the solvent; and δ_s and δ_p, the solubility parameters of the solvent and polymer, respectively. The χ values are given in Table VII. The χ values of the blends are intermediate to those of the components. The interaction parameter decreases with increase of the penetrant size. Contrary to the solvent-uptake order, octane shows the highest interactions with the polymer membrane. This is due to their closer solubility parameter values. The N_{100} membrane shows the lowest χ value among the different membranes.

Effect of Temperature

Diffusion experiments were conducted at four different temperatures, such as 25, 40, 50, and 60°C. The effect of temperature on the diffusion process in N_0, N_{50}, and N_{100} membranes is clearly shown in Figures 22, 23,and 24, respectively. Figure 22 shows that in N_0 the sorption increases with increase of the temperature. Similar behavior was also observed in the other solvents. But in N_{50} (Fig. 23), sorption increases up to 40°C and then slightly decreases. In N_{100}, sorption decreases with increase of the temperature and then it gradually increases (Fig. 24). The maximum sol-

Table VII Interaction Parameter (χ) Values

Solvent	N_0	N_{30}	N_{50}	N_{70}	N_{100}
n-Pentane	0.751	0.6628	0.6099	0.5617	0.4983
n-Hexane	0.626	0.5499	0.5057	0.466	0.4178
n-Heptane	0.603	0.5273	0.4836	0.445	0.3998
n-Octane	0.5393	0.4694	0.4312	0.399	0.3648

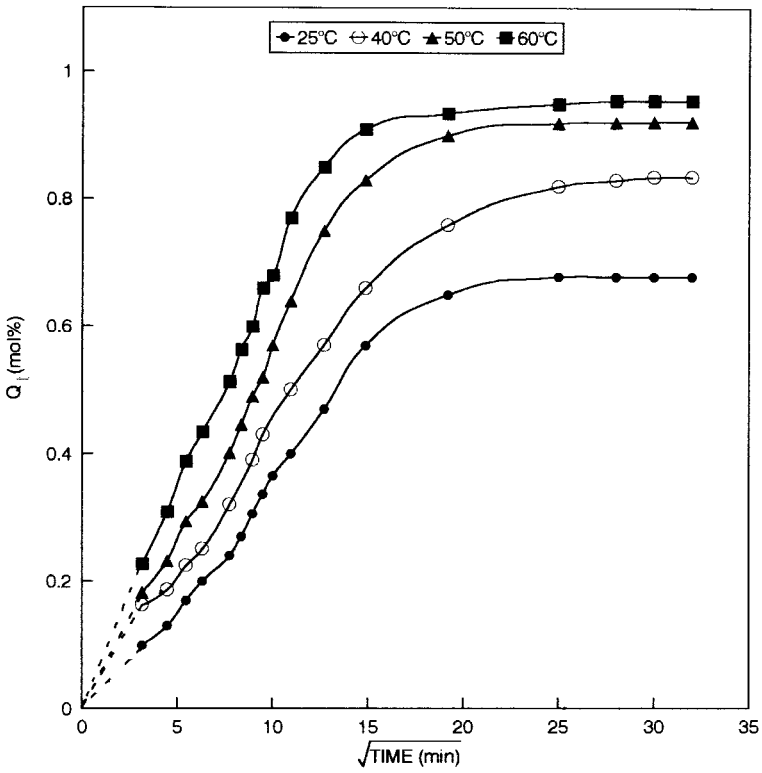

Figure 22 Mol percent octane uptake of N_0 at different temperatures.

vent uptake at higher temperature is lower than that at 25°C. It was found that with an increasing volume fraction of NR the maximum solvent uptake decreases. This can be explained by the heat of sorption calculated using the Van't Hoff relation:

$$\log K_s = \Delta S/2.303R - \Delta H/2.303RT \quad (23)$$

where K_s is the thermodynamic sorption constant; ΔH, the enthalpy of sorption and ΔS, the entropy of sorption. The former quantity is a composite parameter involving both Henry's law and Langmuir-type sorption. Henry's law requires both the formation of a site and the dissolution of the species into that site; this involves an endothermic contribution to the sorption. However, the Langmuir mode involves the sorption by a hole-filling mechanism and thus yields exothermic heat. The estimated values of ΔH and ΔS are given in Table VIII. The correlation coefficient in the determination of ΔH and ΔS is slightly less than 0.99. The ΔH values are positive for N_0, suggesting a Henry's type sorption indicating the endothermic heat of sorption. It is clear from the ΔH values that the sorption changes from Henry's type to Langmuir type with increase in the volume fraction of NR.

Diffusivity, sorptivity, and permeability increase with increase of the temperature irrespective of the solvents used (Tables IV–VI). By using the following Arrhenius relationship, one can estimate the activation energy for diffusion E_D and that for permeation E_P:

$$\log X = \log X_0 - E_x/2.303RT \quad (24)$$

where X stands for either D or P. X_0 represents either D_0 or P_0 and E_x is either E_D or E_P. By the linear regression analysis, the values of E_P and E_D can be determined. The estimated E_D and E_P values are given in Table VIII. The correlation coefficient in the determination of E_D or E_P is slightly less than 0.99. The values are maximum for SBR (N_0) and minimum for NR. The values decrease with increase in the volume fraction of NR. Since $P = DS$, one may also obtain ΔH from the difference $E_P - E_D$, that is:

$$\Delta H = E_P - E_D \quad (25)$$

It is interesting to note that the ΔH estimated from (23) and (25) are almost the same.

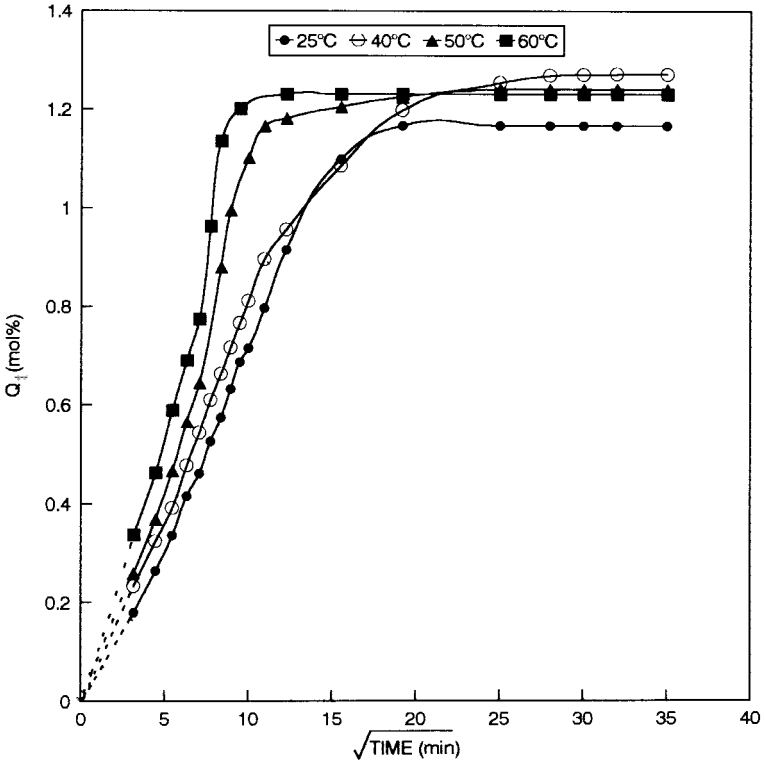

Figure 23 Mol percent octane uptake of N_{50} at different temperatures.

Network Characterization

The investigation of the swelling equilibrium can help to elucidate the structure of the SBR, NR, and SBR/NR polymer networks. Flory and Rehner[23] developed relations for an affine network. In an affine network, the components of each chain vector transform linearly with macroscopic deformation and the junction points are assumed to be embedded in the network without fluctuations. The molar mass between crosslinks (M_c) for the affine model [M_c(aff)] was calculated by the formula[23,31]

$$M_c(\text{aff}) = \frac{-\rho_p V_s \nu_{2c}^{2/3} V_r^{1/3}\left(1 - \frac{\mu}{\nu} V_r^{1/3}\right)}{[\ln(1 - V_r) + V_r + |\chi V_r^2]} \quad (26)$$

where V_s is the molar volume of the solvent, μ and ν are called the number of effective chains and junctions, and V_r is the polymer volume fraction at the swelling equilibrium; ν_{2c}, the polymer volume fraction during crosslinking; and ρ_P, the polymer density. In the phantom network model proposed by James and Guth,[32] chains may move freely through one another. The junction points fluctuate over time around their mean position without being hindered by the presence of the neighboring chains and are independent of deformations. According to the theory, the molar mass between crosslinks for the phantom model [Mc(ph] was calculated by the equation[31,33]

$$M_c(\text{ph}) = \frac{\left(1 - \frac{2}{\phi}\right)\rho_p V_s \nu_{2c}^{2/3} V_r^{1/3}}{-[\ln(1 - V_r) + V_r + \chi V_r^2]} \quad (27)$$

where ϕ is the junction functionality. M_c(aff) and M_c(ph) were compared with the experimentally determined M_c and the values are given in Table IX. It is seen that the M_c values are close to M_c(aff). This suggests that in the highly swollen state the chains in the SBR, NR, and the blends deform affinely.

Comparison with Theory

The experimental diffusion results were compared with theoretical predictions using eq. (11).[27] The experimentally determined values of the diffusion coefficients (D) were substituted in the equation and the representative of the resulting curves are shown in Figures 25 and 26. The

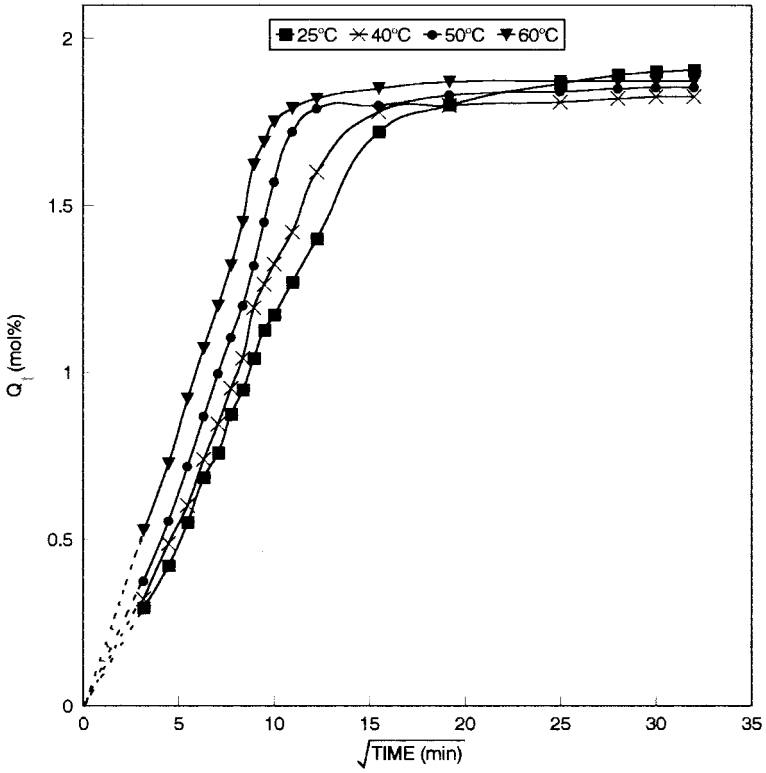

Figure 24 Mol percent octane uptake of N_{100} at different temperatures.

figures represent the behavior of N_0 and N_{100}, respectively. The N_0 and N_{30} membranes exhibit an almost Fickian behavior. However, slight deviation was observed for the N_{50}, N_{70}, and N_{100} samples.

Sorption (*S*)–desorption (*D*)–resorption (*RS*)–redesorption (*RD*)

The sorption process was conducted on polymer samples by the usual swelling method. The swollen samples were then placed in a vacuum oven at a constant temperature for the desorption measurements. These samples were again exposed to the solvent for resorption followed by redesorption. The analysis of the desorption and redesorption studies were conducted similarly to the sorption and resorption process. Sorption, desorption, resorption, and redesorption curves for N_{50} are given in Figure 27. In the desorption experiments, all the samples have the desorption equilibrium greater than the sorption equilibrium. Among different samples, N_{100} has the highest desorption equilibrium and N_0 has the lowest. Blend compositions have intermediate values. This observation might be due to the leaching out of unreacted compounding ingredients from the NR matrix. This is in accordance with the observation that as the volume fraction of NR increases the desorption equilibrium increases. The resorption experiment shows a higher equilibrium uptake in all the cases and it is more predominant for N_{100}. This is due to the increased free volume

Table VIII Thermodynamic and Activation Parameters (Octane)

Parameters	N_0	N_{30}	N_{50}	N_{70}	N_{100}
E_P (kJ/mol)	29.6	20.2	18.37	15.52	14.65
E_D (kJ/mol)	19.67	18.77	17.17	15.78	15.06
$\Delta H(E_P - E_D)$ (kJ/mol)	9.93	1.43	1.12	−0.26	−0.41
ΔS (J mol^{-1} K^{-1})	−11.54	−33.54	−32.9	−37.32	−36.78
ΔH (kJ mol^{-1})	9.04	1.37	1.16	−0.32	−0.378

Table IX Swelling Equilibrium Properties in *n*-Octane

M_c Values	N_0	N_{30}	N_{50}	N_{70}	N_{100}
M_c	2520	3774	3996	4563	6725
M_c (aff)	2348	3519	3729	4261	6288
M_c (ph)	1174	1759	1864	2130	3144

generated by the leaching out of additives during the sorption–desorption experiments. The redesorption equilibrium is almost similar to the resorption equilibrium, indicating no further leaching out of additives.

Degree of Crosslinking

In a crosslinked system, both physical and chemical crosslinks are formed; physical crosslinks consist of chain entanglements which vary according to the stress developed in the system. But the chemical crosslinks develop from the chemical bonds connecting the polymer segments. The degree of crosslinking can be measured from the swelling, stress–strain, and dynamic mechanical analysis.

One can use the storage modulus data for determining the degree of crosslinking (n_2) from dynamic mechanical analysis and this was done by using the following relation[34]:

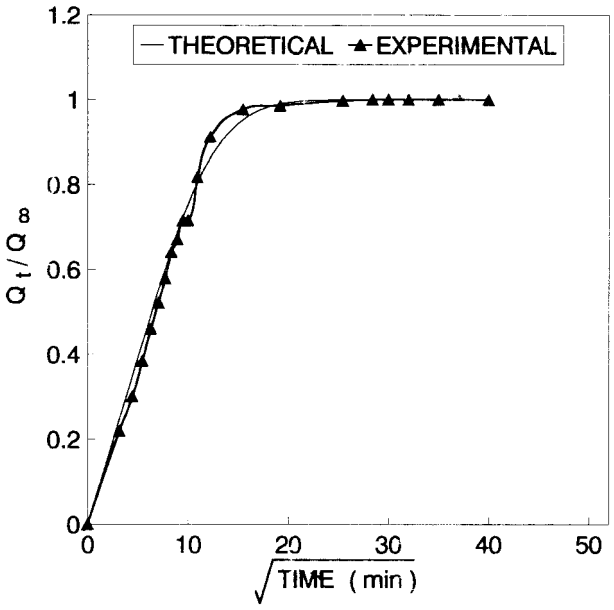

Figure 25 Comparison of experimental diffusion results of N_0 with that of theoretical prediction.

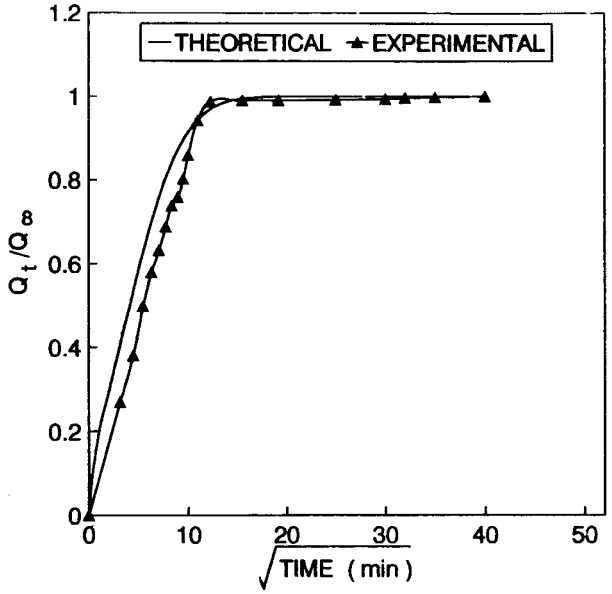

Figure 26 Comparison of experimental diffusion results of N_{100} with that of theoretical prediction.

$$n_2 = E'/6RT \tag{28}$$

where E' is the storage modulus estimated from the plateau regions of E' versus the temperature curve; R, the universal gas constant; and T, the absolute temperature. From the stress–strain measurements, one has to use the following relation for determining the degree of crosslinking[35]:

$$n_3 = \frac{\tau}{RT(\alpha - 1/\alpha^2)V_r^{1/3}} \tag{29}$$

where τ is the stress; α, the extension ratio; and V_r, the volume fraction of the polymer in the solvent swollen sample.

The degrees of crosslinking determined by using eqs. (9), (28), and (29) are given in Table X. They are complementary to each other. The degree of crosslinking calculated from different methods suggests that the maximum number of crosslinks per unit volume is possessed by the N_0 sample, and the lowest, by the N_{100} sample. The blends have intermediate values.

CONCLUSIONS

The effect of the blend composition on the transport behavior and mechanical and dynamic mechanical properties of SBR/NR blends was investigated. SEM studies established the heterophase

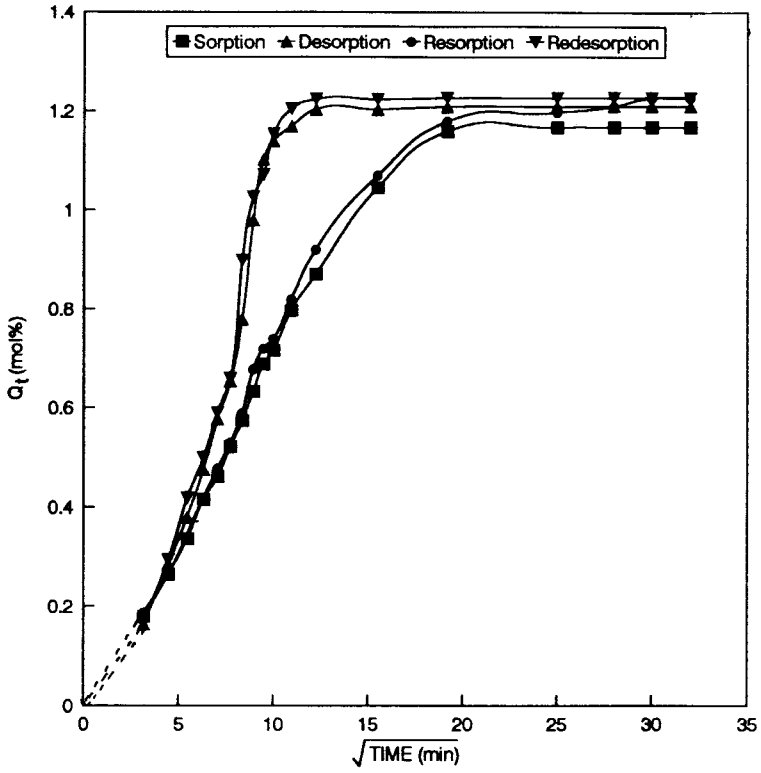

Figure 27 Sorption–resorption–resorption–redesorption of N_{50} in *n*-octane.

nature of the blend. The 50/50 and 30/70 SBR/NR blend compositions show a cocontinuous morphology. DMA indicates that SBR/NR blends are incompatible, as shown by the presence of two relaxation peaks corresponding to the T_g's of SBR and NR. As the concentration of NR increases, the storage modulus of the system decreases, while the loss modulus and tan δ increase. The mechanical properties of the blends are also intermediate to those of the homopolymers. The properties of the swollen samples are largely reduced due to the high rubber–solvent interaction during swelling. Further, the various transport parameters established the heterophase nature of the blend. The diffusion coefficient, permeation coefficient, and sorption coefficient are intermediate to those of the individual components. Various composite models were used to fit the experimental permeation data. The Robeson model was found to fit the experimental values for the N_{50} composition. The enthalpy of sorption shows that Henry's law-type sorption operates in SBR, which changes to Langmuir-type sorption with increase in the volume fraction of NR. Network characterization indicates that the crosslinks in the SBR/NR blends deform in an affine manner. The degree of crosslinking significantly influences different properties. It was found that the degree of crosslinking determined from the swelling, tensile stress–strain, and dynamic mechanical analysis are in the same order. However, the degree of crosslinking calculated from dynamic mechanical analysis is considerably lower than that of the other methods.

Table X Degree of Crosslinking × 10^4 mol/cc

Sample	n_1	n_2	n_3
N_0	1.98	1.09	1.83
N_{30}	1.33	0.79	1.81
N_{50}	1.25	0.74	1.80
N_{70}	1.09	0.72	1.09
N_{100}	0.74	0.71	0.92

n_1, from swelling measurements; n_2, from dynamic mechanical analysis; n_3, from stress–strain measurements.

One of the authors (S. C. G.) is grateful to Ms. Asaletha, Lecturer, STAS, for her valuable help during preparation of the manuscript.

REFERENCES

1. Hopfenberg, H. B.; Paul, D. R. Polymer Blends; Paul, D. R.; Newman, S., Eds.; Academic: New York, 1978; Chapter 10.

2. Paul, D. R. J Membr Sci 1984, 18, 75.
3. Chiou, J. S.; Paul, D. R. J Appl Polym Sci 1986, 32, 2897, 4793.
4. Odani, H.; Uchikura, M.; Ogino, Y.; Kurata, M. J Membr Sci 1983, 15, 193.
5. Cabasso, I.; Jagur-Grodziski, J.; Vofsi, D. J Appl Polym Sci 1974, 18, 2117.
6. Schori, E.; Jagur-Grodziski, J. J Appl Polym Sci 1976, 20, 773.
7. Aminabhavi, T. M.; Phyde, H. T. S. J Appl Polym Sci 1995, 57, 1491.
8. Aminabhavi, T. M.; Phyde, H. T. S. Eur Polym J 1996, 32, 1117.
9. Johnson, T.; Thomas, S. J Mater Sci 1999, 34, 3221.
10. Varghese, H.; Bhagawan, S. S.; Thomas, S. J Polym Sci Part B Polym Phys, in press.
11. Asaletha, R.; Kumaran, M. G.; Thomas, S. Polym Polym Comp 1998, 6, 357.
12. George, S.; Varghese, K. T.; Thomas, S. Polymer, in press.
13. Harogoppad, S. B.; Aminabhavi, T. M. J Appl Polym Sci 1991, 42, 2329.
14. Franson, M.; Peppas, N. A. J Appl Polym Sci 1983, 28, 1299.
15. Moon, Y. D.; Lee, Y. M. J Appl Polym Sci 1994, 51, 945.
16. Danesi, C. S.; Porter, R. S. Polymer 1978, 19, 448.
17. Wisme, C.; Maria, G.; Monge, P. Eur Polym J 1985, 21, 479.
18. George, S.; Prasnnakumar, L.; Koshy, P.; Varughese, K. T.; Thomas, S. Mater Lett 1996, 26, 51.
19. Kunori, T.; Geil, P. H. J Macromol Sci Phys B 1980, 18, 135.
20. Kerner, E. H. Proc Phys Soc 1956, 696, 808.
21. Southern, E.; Thomas, A. G. Trans Faraday Soc 1967, 63, 1913.
22. Bhowmick, A. K.; Stephens, H. L. Handbook of Elastomers; Marcel Dekker: New York, 1988.
23. Flory, P. J. Principles of Polymer Chemistry; Cornell University: Ithaca, NY, 1953.
24. Aithal, U. S.; Aminabhavi, T. M. J Chem Ed 1990, 67, 82.
25. Froething, P. E.; Koenhen, D. M.; Bantjes, A.; Smolders, C. A. Polymer 1976, 17, 835.
26. Lee, Y. M.; Bourgeois, D.; Belfort, G. Membr Sci 1989, 44, 161.
27. Crank, J. S. The Mathematics of Diffusion, 2nd ed.; Clarendon: Oxford, 1975.
28. Harogoppad, S. B.; Aminabhavi, T. M. Macromolecules 1991, 24, 2598.
29. Brown, W. K.; Jenkins, R. B.; Park, G. S. J Appl Polym Sci Polym Symp 1973, 41, 45.
30. Takahashi, S. J Appl Polym Sci 1983, 28, 2847.
31. Treloar, L. R. G. The Physics of Rubber Elastivity; Clarendon: Oxford, 1975.
32. James, H. M.; Guth, E. J Chem Phys 1947, 15, 669.
33. Mark, J. E.; Erman, B. Rubberlike Elasticity, A Molecular Primer; Wiley: New York, 1985.
34. Hagen, R.; Salmen, L.; Stenberg, B. J Polym Sci Part B Polym Phys 1996, 34, 1997.
35. Mark, H. F.; Bikales, N. M.; Overberg, G. G.; Menges, G. (Eds.). Encyclopedia of Polymer Science and Engineering; Wiley: New York, 1986; Vol. 4, p 356.